Title

Dynamics of Cation-Induced Conformational Changes in Nanometer-Sized Uranyl Peroxide Clusters

Journal

Inorganic Chemistry, 59(4)

ISSN

0020-1669

Authors

Dembowski, Mateusz
Pilgrim, Corey D
Hickam, Sarah
et al.

Publication Date

2020-02-17

DOI

10.1021/acs.inorgchem.9b03390

Peer reviewed

Inorganic Chemistry

pubs.acs.org/IC Article

Dynamics of Cation-Induced Conformational Changes in Nanometer-Sized Uranyl Peroxide Clusters

Mateusz Dembowski, Corey D. Pilgrim, Sarah Hickam, Tyler Spano, Dallas Hamlin, Allen G. Oliver, William H. Casey, and Peter C. Burns*

Cite This: *Inorg. Chem.* 2020, 59, 2495−2502 Read Online

ACCESS | Metrics & More | Article Recommendations | Supporting Information

ABSTRACT: Conformational changes of the pyrophosphate (Pp)-functionalized uranyl peroxide nanocluster $[(UO_2)_{24}(O_2)_{24}(P_2O_7)_{12}]^{48-}$ ($\{U_{24}Pp_{12}\}$), dissolved as a Li/Na salt, can be induced by the titration of alkali cations into solution. The most symmetric conformer of the molecule has idealized octahedral (O_h) molecular symmetry. One-dimensional ^{31}P NMR experiments provide direct evidence that both K^+ and Rb^+ ions trigger an O_h-to-D_{4h} conformational change within $\{U_{24}Pp_{12}\}$. Variable-temperature ^{31}P NMR experiments conducted on partially titrated $\{U_{24}Pp_{12}\}$ systems show an effect on the rates; increased activation enthalpy and entropy for the D_{4h}-to-O_h transition is observed in the presence of Rb^+ compared to K^+. Two-dimensional, exchange spectroscopy ^{31}P NMR revealed that magnetization transfer links chemically unique Pp bridges that are present in the D_{4h} conformation and that this magnetization transfer occurs via a conformational rearrangement mechanism as the bridges interconvert between two symmetries. The interconversion is triggered by the departure and reentry of K (or Rb) cations out of and into the cavity of the cluster. This rearrangement allows Pp bridges to interconvert without the need to break bonds. Cs ions exhibit unique interactions with $\{U_{24}Pp_{12}\}$ clusters and cause only minor changes in the solution ^{31}P NMR signatures, suggesting that O_h symmetry is conserved. Single-crystal X-ray diffraction measurements reveal that the mixed Li/Na/Cs salt adopts D_{2h} molecular symmetry, implying that while solvated, this cluster is in equilibrium with a more symmetric form. These results highlight the unusually flexible nature of the actinide-based $\{U_{24}Pp_{12}\}$ and its sensitivity to countercations in solution.

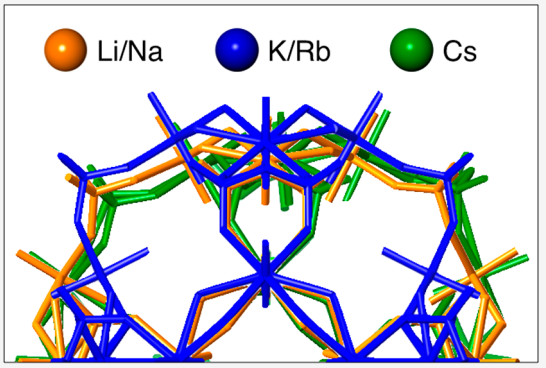

INTRODUCTION

Uranyl peroxide nanoclusters are a rapidly expanding subclass of polyoxometalates (POMs).[1] Their anionic nature,[2] high aqueous solubility,[3,4] and chemical robustness paired with the tendency to form highly symmetrical, hollow-cage structures are reminiscent of transition-metal Keplerates.[5] Notably, both classes of macroanions are characterized by the presence of chemically inert, surface passivating -yl O atoms, albeit in different spatial orientations.[6] Group V and VI transition metals in their highest oxidation states are bound by one, or two, cis-oriented -yl O atoms that promote the assembly of structures ranging from prototype Lindqvist and Keggin ions to core−shell Keplerate and Molybdenum Blue ions.[6−8] Because of the cis orientation of -yl O atoms, the cavity of core−shell transition-metal POMs incorporates additional ligands that affect the reactivity of its surface.[7,9] Hexavalent U, in contrast, is bound by two trans-oriented -yl O atoms that passivate both the outside and inside of the resulting core−shell clusters, precluding the incorporation of supplementary species.[10] The diverse structural family of transition-metal POMs shows potential applications in medicine,[11] catalysis,[12] and materials science,[13] while uranyl peroxide nanoclusters may be important in advanced nuclear cycles and in the environmental chemistry of actinides.[14,15]

Despite their relatively recent discovery, over 70 unique structures of uranyl peroxide nanoclusters have now been reported.[10] A significant fraction of these nanoclusters incorporate pyrophosphate (Pp) or methylenediphosphonate (PCP) ligands. In contrast to their transition-metal counterparts, the synthesis of Pp-functionalized uranyl peroxide nanoclusters is not impeded by acid-promoted hydrolysis of Pp ligands.[16,17] Hence, the ions of these clusters can be used to study the assembly and solution dynamics of uranyl clusters using ^{31}P NMR.[18−20] In addition to verifying the stability of Pp-functionalized uranyl peroxide nanoclusters in solution, ^{31}P NMR spectroscopy revealed the existence of two unique conformations of $[(UO_2)_{24}(O_2)_{24}(P_2O_7)_{12}]^{48-}$ ($\{U_{24}Pp_{12}\}$). NMR experiments demonstrated that the two chemically

Received: November 19, 2019
Published: February 4, 2020

https://dx.doi.org/10.1021/acs.inorgchem.9b03390
Inorg. Chem. 2020, 59, 2495−2502

unique Pp environments are present in its D_{4h} conformation transfer magnetization dynamically.[19−21] Single-crystal diffraction studies of $\{U_{24}Pp_{12}\}$ showed that different conformations of this cluster (O_h vs D_{4h}) are likely associated with the presence of different alkali-metal cations in their cavities.[20] A subsequent isothermal titration calorimetry study noted that the introduction of K^+ or Rb^+ into the O_h $\{U_{24}Pp_{12}\}$ system led to a strong endothermic process that was interpreted to indicate binding of these cations within the cluster's cavity and a change to the D_{4h} molecular symmetry.[22] Because no bonds are broken, this change in symmetry is subsequently referred to as *conformational rearrangement*.

The importance of countercations in affecting the POM structure and stabilities has long been recognized.[23,24] One of the fundamental roles of these ions in solution is controlling the solubility of POMs. With chaotropic anions, the POM solubility increases in the presence of small, strongly solvated alkali metals (Li^+ or Na^+). This is the case for acid-stable V-, Mo-, and W-based clusters.[23] There are, however, exceptions to this "normal" solubility behavior in the form of alkali-stable Nb- and Ta-POMs, which exhibit high, anomalous solubility in the presence of large alkali (Cs^+) or tetramethylammonium (TMA^+) ions.[25−27] Recently, it was demonstrated that the solubility of uranyl peroxide-based POMs, the stability fields of which span both acidic and alkaline conditions, follow "normal" trends with Li and Na salts displaying significantly higher solubilities than larger alkali-metal salts.[3,4] Additionally, cations play a commanding role during the synthesis of POMs, enabling the isolation of reactive lacunary species or enantiomerically pure clusters.[28,29] In uranyl peroxide-based POMs, the role of cations as structure-directing agents was proposed on the basis of experimentally observed trends and since has been a topic of several subsequent theoretical studies.[30−32] The introduction of excess salt to solutions containing transition-metal or uranyl peroxide-based POMs results in the cation-promoted self-assembly of these anions into supramolecular "blackberry" structures.[33−35] The diversity and multiplicity of anion−cation interactions observed in POM systems is a topic of ongoing studies with potential implications in catalysis, electronics, magnetism, and environmental remediation.[14,36−38]

Herein, we exploit the presence of the NMR-active ligand in the structure of $\{U_{24}Pp_{12}\}$ to directly observe the K^+- and Rb^+-induced O_h-to-D_{4h} conformation change prior to crystallization. We also perform variable-temperature (VT) NMR experiments to gain insight into the energetics of counterion interactions with the cluster. Exchange spectroscopy (EXSY) NMR experiments were conducted to elucidate the mechanism of magnetization transfer between two chemically unique Pp bridges that are present in the D_{4h} conformation of $\{U_{24}Pp_{12}\}$. A supplementary single-crystal X-ray diffraction study of the Cs^+-containing system revealed a new D_{2h} conformation of $\{U_{24}Pp_{12}\}$, which further emphasizes the remarkable flexibility of this cluster.

EXPERIMENTAL SECTION

Warning! *All experiments were carried out using isotopically depleted U by trained personnel in laboratories designed for handling radioactive materials.*

General Considerations. Uranyl nitrate hexahydrate ($UO_2(NO_3)_2{\cdot}6H_2O$; International Bio-Analytical Industries, Inc.), hydrogen peroxide (H_2O_2, 30% aqueous solution; EMD Millipore), sodium pyrophosphate ($Na_4P_2O_7$; Spectrum), lithium hydroxide monohydrate ($LiOH{\cdot}H_2O$; EMD Millipore), oxalic acid ($H_2C_2O_4$; Sigma-Aldrich), potassium nitrate (KNO_3; BDH), rubidium nitrate ($RbNO_3$; Sigma-Aldrich), cesium nitrate ($CsNO_3$; Alfa Aesar), and deuterium oxide (98% D_2O; Cambridge Isotope Laboratories, Inc.) were purchased from commercial suppliers and used as received.

Pp-functionalized uranyl peroxide nanoclusters are abbreviated as $\{U_nPp_m\}$, where n corresponds to the number of $[(UO_2)(O_2)]$ units and m represents the number of Pp ($P_2O_7^{4-}$) bridges, respectively. Synthesis of the Li/Na salt of $\{U_{24}Pp_{12}\}$ was carried out in accordance with previously described procedures.[20] The identity and purity of the synthesized material was confirmed via inductively coupled plasma optical emission spectroscopy and ^{31}P NMR spectroscopy (see the Supporting Information).

$\{U_{24}Pp_{12}\}$ Synthesis. $Li_{48-x}Na_x[(UO_2)_{24}(O_2)_{24}(P_2O_7)_{12}]{\cdot}nH_2O$ (Li:Na ≈ 3:1) was synthesized according to the procedure reported in the literature.[20] Briefly, 10 mL of 0.5 M $UO_2(NO_3)_2$, 10 mL of 30% H_2O_2, and 12.5 mL of 0.2 M $Na_4P_2O_7$ were combined in a 100 mL beaker, resulting in the rapid precipitation of a pale-yellow solid. The resulting suspension was titrated using 2.38 M LiOH until pH = 9.3 was reached, leading to dissolution of the solid, effervescence, and a color change to dark orange. The pH of the solution was then adjusted, using 0.5 M $H_2C_2O_4$, to pH = 7 over a period of several days until no further change in the pH was noted. The beaker was left uncovered to facilitate evaporation. Orange crystals formed within 4 weeks.

Cation Titrations. Titrations were carried out on 1 mL aliquots of the stock solution prepared by the dissolution of crystalline Li/Na salt of $\{U_{24}Pp_{12}\}$ (20 mg/mL, $[\{U_{24}Pp_{12}\}]$ = 1.6 mM). Between 5 and 40 μL of a 0.25 M KNO_3, $RbNO_3$, or $CsNO_3$ solution was added to 1 mL aliquots of a 1.6 mM $\{U_{24}Pp_{12}\}$ solution, corresponding to 0.76−6.11 mol equiv. The resulting mixtures were vortexed and capped. Because of cation-induced precipitation of $\{U_{24}Pp_{12}\}$, the range of experimental conditions considered in this study was limited to $0 < r < 6.1$, where r is defined as the cation-to-cluster ratio. The stock solution used for titration experiments was prepared using a 1:5 D_2O/H_2O mixture, allowing for signal locking and shimming. NMR data were collected 24 h after the introduction of cations into the stock solution. The stability of the solutions, up to 30 days, was confirmed by means of ^{31}P NMR spectroscopy and electrospray ionization mass spectrometry (ESI-MS; see Supporting Information). Crystals used for structure determination purposes were obtained by the slow evaporation of titrated stock solutions ($r > 3.1$) over a period of 2 weeks. Unfortunately, the K^+, Rb^+, and Cs^+ systems produced small quantities (ca. 5% based on U) of crystalline material only suitable for single-crystal X-ray diffraction. Prolonged evaporation of these systems led to the extensive precipitation of a microcrystalline material, precluding meaningful analyses of the bulk.

Single-Crystal X-ray Diffraction. Crystals obtained through a slow evaporation process were transferred, along with a small quantity of mother liquor, into oil and mounted on cryoloops. A stream of nitrogen gas afforded a data collection temperature of 110 K. A full sphere of data were collected for each crystal using a Bruker APEX II Quazar diffractometer equipped with a microfocus tube with multilayer monochromated Mo Kα X-rays, 0.5° frame widths (in ω), and exposure times of 10−30 s. The Bruker *APEX III* software package was used for data integration. Absorption corrections, including corrections for Lorentz, polarization, and background effects, were applied using *SADABS*.[39] The *SHELXTL* suite was used for structure solution and refinement.[40,41] Establishing the positions of the H atoms in the reported structures was not attempted. Crystallographic information is summarized in Table S1.

NMR Spectroscopy. One-dimensional (1D), VT, and two-dimensional (2D) EXSY ^{31}P NMR spectra were collected on a 500 MHz Varian INOVA spectrometer (11.57 T), using a 56 dB power level attenuation, a 14.8 μs pulse length, and a 5 s relaxation delay (d1). 1D spectra were collected at 25 °C and 64 scans. Prior to data collection, samples were allowed to equilibrate for 5 min after the instrument reached the desired temperature. EXSY data were acquired on a stationary sample (no spin) at 25 °C by varying the

https://dx.doi.org/10.1021/acs.inorgchem.9b03390
Inorg. Chem. 2020, 59, 2495−2502

mixing time (d8) from 5 to 300 ms. ^{31}P NMR chemical shifts are reported with respect to neat H_3PO_4 (δ = 0 ppm).

Characterization Data. Additional crystallographic data are available in Tables S2–S13 and in CIF format.

RESULTS AND DISCUSSION

The Pp-functionalized uranyl peroxide nanocluster $\{U_{24}Pp_{12}\}$ is one of the most studied actinide–peroxide complexes, for reasons discussed above.[20−22] Prior findings demonstrated that $\{U_{24}Pp_{12}\}$ can assume at least two unique conformations corresponding to an idealized O_h (Li/Na salt, δ = 3.80 ppm) or D_{4h} (Na/K salt, δ = 3.45/4.28 ppm) molecular symmetry.[19,20] Herein, solutions containing solvated Li/Na salt of $\{U_{24}Pp_{12}\}$ ($[\{U_{24}Pp_{12}\}]$ = 1.6 mM) were titrated using 0.25 M KNO_3, $RbNO_3$, and $CsNO_3$ solutions. 1D ^{31}P NMR spectra representing different stages of the titration process are summarized in Figures 1 (KNO_3 and $RbNO_3$) and S1 ($CsNO_3$) and Table 1.

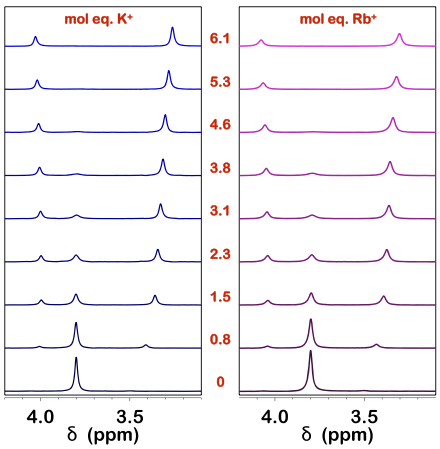

Figure 1. ^{31}P NMR spectra showing changes during a progressive titration of a 1.6 mM solution of Li/Na salt of $\{U_{24}Pp_{12}\}$ with 0.25 M KNO_3 (left) and 0.25 M $RbNO_3$ (right).

The results of 1D ^{31}P NMR experiments were interpreted based on changes to the (i) signal intensities and positions (K^+ and Rb^+; Figure 1) and (ii) signal position (Cs^+; Figure S1). Titration of the stock solution containing Li/Na $\{U_{24}Pp_{12}\}$ with KNO_3 results in gradual replacement of the original signal that was located at 3.80 ppm (δ_1) with two new ones at 3.41 ppm (δ_2) and 4.01 ppm (δ_3). The newly emerged signals, assigned to the $\{U_{24}Pp_{12}\}$ cluster in its D_{4h} molecular conformation, shift progressively upfield (K^+, δ_2 from 3.41 to 3.26 ppm) and downfield (K^+, δ_3 from 4.01 to 4.03 ppm) with increasing K^+ concentration (Figure 1 and Table 1). The ratio of the new signal intensities (δ_2 and δ_3) remains constant throughout the titration process (ca. 2:1), consistent with the NMR data reported for the mixed Na/K salt of $\{U_{24}Pp_{12}\}$ and supporting their initial assignment.[19,21] The addition of Rb^+ into the Li/Na $\{U_{24}Pp_{12}\}$ system yields similar results, with the extents of the upfield (Rb^+, δ_2 from 3.43 to 3.31 ppm) and downfield (Rb^+, δ_3 from 4.04 to 4.08 ppm) shifts varying slightly from those observed in the K^+ system. These new signals are assigned to the cluster in the D_{4h} conformation. Both systems undergo complete O_h-to-D_{4h} transformation as the cluster to the K^+/Rb^+ ratio in solution reaches ca. 1:6 (Table 1). For comparison, a prior isothermal titration calorimetry study produced the same ratio for Rb^+ as the titrant but a higher 1:8 ratio for K^+.[22] Slow evaporation of solutions titrated with KNO_3 and $RbNO_3$ (for K^+/Rb^+ mol equiv $\geq$ 3.1) resulted in the formation of crystals that were suitable for single-crystal X-ray diffraction studies. Diffraction results confirmed the proposed D_{4h} molecular symmetry of $\{U_{24}Pp_{12}\}$ in both the K^+ $Li_{48-x-y}Na_xK_y[(UO_2)_{24}(O_2)_{24}(P_2O_7)_{12}]\cdot nH_2O$ (**1**) and Rb^+ $Li_{48-x-y}Na_xRb_y[(UO_2)_{24}(O_2)_{24}(P_2O_7)_{12}]\cdot nH_2O$ (**2**) systems (Figure 2). The crystallographic results, including unit cell parameters, and structure descriptions are available in the Supporting Information.

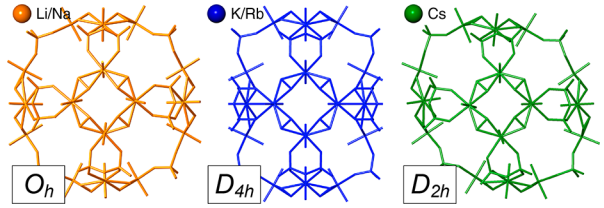

Figure 2. Graphical representation of the $\{U_{24}Pp_{12}\}$ cluster as (left) a Li/Na salt showing idealized O_h symmetry, (center) a Li/Na/K or Rb salt showing idealized D_{4h} symmetry, and (right) a Li/Na/Cs salt showing idealized D_{2h} symmetry.

Titration of the Li/Na $\{U_{24}Pp_{12}\}$ system with Cs^+, for comparison to systems with K^+ or Rb^+, does not cause a significant change in the ^{31}P NMR spectra. While the chemical shift δ_1 shifts upfield from 3.80 to 3.51 ppm as a function of the added Cs^+, the number of ^{31}P NMR resonances remains unchanged (Figures S1 and S4 and Table 1). The presence of a single ^{31}P NMR resonance is interpreted to indicate that

Table 1. Summary of the Chemical Shift (δ_x) and Signal Population (Percentage of Intensity) Changes during Titration of a 1.6 mM Solution of Li/Na Salt of $\{U_{24}Pp_{12}\}$ with Equivalents of 0.25 M KNO_3, $RbNO_3$, and $CsNO_3$

	K			Rb			Cs
mol equiv	δ_1 (% int)	δ_2 (% int)	δ_3 (% int)	δ_1 (% int)	δ_2 (% int)	δ_3 (% int)	δ_1 (% int)
0	3.80 (100.0)	N/A	N/A	3.80 (100.0)	N/A	N/A	3.80 (100.0)
0.8	3.80 (80.4)	3.41 (13.5)	4.01 (6.1)	3.80 (78.9)	3.43 (14.7)	4.04 (6.4)	3.78 (100.0)
1.5	3.80 (46.8)	3.36 (35.3)	4.00 (17.9)	3.80 (47.2)	3.40 (35.4)	4.04 (17.4)	3.73 (100.0)
2.3	3.80 (34.4)	3.34 (43.8)	4.00 (21.8)	3.80 (32.3)	3.38 (45.3)	4.05 (22.4)	3.67 (100.0)
3.1	3.80 (23.1)	3.33 (51.3)	4.00 (25.6)	3.80 (22.6)	3.37 (51.8)	4.05 (25.6)	3.60 (100.0)
3.8	3.80 (14.9)	3.31 (56.6)	4.00 (28.5)	3.80 (17.6)	3.37 (55.1)	4.06 (27.3)	3.51 (100.0)
4.6	3.79 (9.3)	3.30 (60.2)	4.01 (30.5)	3.80 (9.0)	3.36 (61.1)	4.07 (29.9)	N/A
5.3	3.79 (5.2)	3.28 (63.2)	4.02 (31.6)	3.80 (2.5)	3.32 (64.9)	4.07 (32.6)	N/A
6.1	N/A	3.26 (66.2)	4.03 (33.8)	N/A	3.31 (67.2)	4.08 (32.8)	N/A

https://dx.doi.org/10.1021/acs.inorgchem.9b03390
Inorg. Chem. 2020, 59, 2495−2502

$\{U_{24}Pp_{12}\}$ retains its original O_h molecular symmetry in solution. This persistence is consistent with an isothermal calorimetry study suggesting that Cs ions are too large to form strong cation−oxygen interactions with the inner windows of $\{U_{24}Pp_{12}\}$. However, the observed changes in the chemical shifts imply interaction between the Cs^+ ions and Pp bridges. The slow evaporation of solutions titrated with $CsNO_3$ (for Cs^+ mol equiv ≥ 2.3) afforded crystals that were suitable for single-crystal X-ray diffraction. The structure solution revealed Cs ions present both inside and outside the $\{U_{24}Pp_{12}\}$ cluster exhibiting idealized D_{2h} molecular symmetry (Figure 2), suggesting that Cs^+ can, in fact, pass through the pores of the solvated $\{U_{24}Pp_{12}\}$.

The discrepancy between the observed and anticipated numbers of ^{31}P NMR signals for the Li/Na/Cs $\{U_{24}Pp_{12}\}$ (obs., 1; ant., 3; 1:4:1 intensity ratio) is interpreted to indicate rapid interconversion between different conformations of $\{U_{24}Pp_{12}\}$ via a symmetrical (O_h) intermediate with the departure from the original chemical shift (δ_1 = 3.80 ppm) attributed to a population-weighted average of the chemical shifts of the two conformations (O_h vs D_{2h}). Note: the exchange between the O_h and D_{4h} conformations observed in the systems titrated with K^+ and Rb^+ is relatively slow with respect to NMR experiment time scales, resulting in distinct, sharp signals. A similar hypothesis was evoked in a prior NMR study of the D_{4h} $\{U_{24}Pp_{12}\}$ cluster that demonstrated a change in the magnetic environment between the two unique Pp bridges at room temperature and their convergence at elevated temperatures. The exchange was proposed to occur via a more symmetrical (O_h) intermediate and represented the only viable path that did not include bond dissociation.[19] The crystallographic results, including unit cell parameters, and structure description of the $Li_{48-x-y}Na_xCs_y[(UO_2)_{24}(O_2)_{24}(P_2O_7)_{12}]\cdot nH_2O$ (**3**) are available in the Supporting Information.

The set of conformations observed for this large actinide anion, paired with ^{31}P NMR results showing various degrees of in situ conformational interchange, highlight the flexible nature of the $\{U_{24}Pp_{12}\}$ cluster and its adaptability to different guest ions. A comparison of the $\{U_6P_3O_9\}$ pores that are present in $\{U_{24}Pp_{12}\}$ and that control the passage of ions and solvent molecules between its cavity and the interstitial space reveals significant deformations. Notably, the pore size, as defined by the triangular area between peroxide O atoms located near the pore entrance (Figure 3), changes from 25.24 Å^2 in the Li/Na salt to 19.29 and 24.91 Å^2 upon the incorporation of K/Rb and Cs ions, respectively, a maximum pore-size change of ca. 24%.

It is important to emphasize that solvated $\{U_{24}Pp_{12}\}$ reacts to the introduction of different cations into the system in a fashion unlike any other POM described to date. The closest structural relative of $\{U_{24}Pp_{12}\}$ with similar behavior are molecules within the family of transition-metal Keplerates, which are much larger than the actinyl peroxide described here. In a series of studies, the affinity of $[\{(Mo)Mo_5O_{21}(H_2O)_6\}_{12}\{Mo_2O_4(ligand)\}_{30}]^{42-}$ $\{Mo_{132}\}$ toward a variety of cationic species revealed specific interactions at unique areas of the transition-metal capsule, which remains rigid.[42,43] This indifference toward cations among the Keplerates contrasts sharply with the conformational rearrangement observed here for $\{U_{24}Pp_{12}\}$, where cluster−cation interactions cause significant deformation.

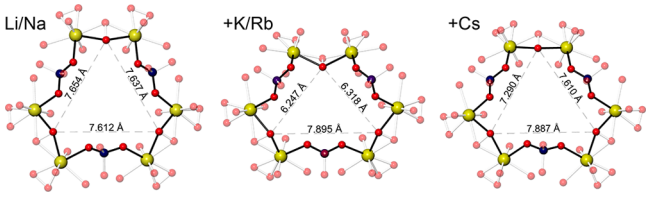

Figure 3. Ball-and-stick representation of the chosen $\{U_6P_3O_9\}$ pores present in different salts of $\{U_{24}Pp_{12}\}$, highlighting changes in the nearest peroxide-to-peroxide distances. Yellow, purple, and red spheres represent U, P, and O atoms, respectively. Cations and water molecules are omitted for clarity.

To gain insight into the energetics of conformational changes of the $\{U_{24}Pp_{12}\}$ cluster, VT ^{31}P NMR experiments were performed on Li/Na $\{U_{24}Pp_{12}\}$ solutions containing 1.5 mol equiv of K^+ (or Rb^+). The reference (T = 298 K) 1D ^{31}P NMR spectrum is characterized by three resonances that correspond to a mixture of the $\{U_{24}Pp_{12}\}$ cluster in its O_h (δ_1 = 3.80 ppm) and D_{4h} (δ_2 = 3.36 ppm and δ_3 = 4.00 ppm) symmetry in ca. 1:1 ratio (Table 1). Increasing the temperature from 298 to 338 K (ΔT = 2.5 K) resulted in regular broadening and eventual coalescence of all signals, indicating more rapid interconversion between the three sites (Figures 4 and S8). The peak widths obtained at different stages of the heating process were estimated using a Lorentzian line-fitting procedure (*MestReNova*, version 10), and the rate coefficient of the exchange, k_{ex}, was estimated using the following equation:

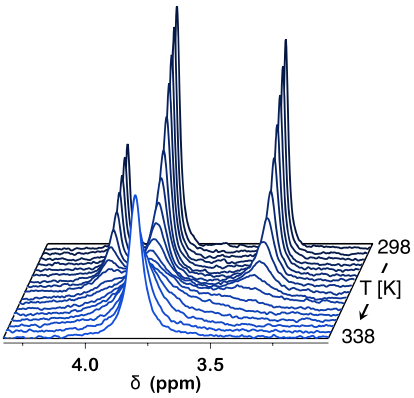

Figure 4. VT ^{31}P NMR spectra showing the gradual broadening and coalescence of $\{U_{24}Pp_{12}\}$ + 1.5 mol equiv of K^+ signals as a function of the temperature.

$$\frac{1}{\pi T_2^*} + k_{ex} = \omega_{fwhm}$$

where $\frac{1}{\pi T_2^*}$ corresponds to the intrinsic line width of the peak and the measured full width at half-maximum (fwhm) at each temperature. The intrinsic line width of the peaks was estimated using the width of a well-shimmed sample at 298 K because only minor broadening was noted in all peaks below 303 K. The data from all three sites were fit using the Eyring−Polanyi equation:[44,45]

$$k_{ex} = \frac{k_B T}{h} e^{-\Delta G^{\ddagger}/RT} \rightarrow \ln\left(\frac{k_{ex}}{T}\right) = \ln\left(\frac{k_B}{h}\right) - \frac{\Delta G^{\ddagger}}{RT}$$
$$= -\left(\frac{1}{T}\right)\left(\frac{\Delta H^{\ddagger}}{R}\right) + \left[\frac{\Delta S^{\ddagger}}{R} + \ln\left(\frac{k_B}{h}\right)\right]$$

https://dx.doi.org/10.1021/acs.inorgchem.9b03390
Inorg. Chem. 2020, 59, 2495−2502

where k_B is Boltzmann's constant, h is Planck's constant, R is the gas constant, T is the temperature in Kelvin, and $X^{\ddagger}$ corresponds to the activation quantities for Gibbs' free energy ($\Delta G^{\ddagger}$), enthalpy ($\Delta H^{\ddagger}$), and entropy ($\Delta S^{\ddagger}$).

The Eyring–Polanyi plots obtained from the $\{U_{24}Pp_{12}\}$ system titrated with 1.5 mol equiv of K^+ and Rb^+ are shown in Figure 5. From regression of the data, the activation

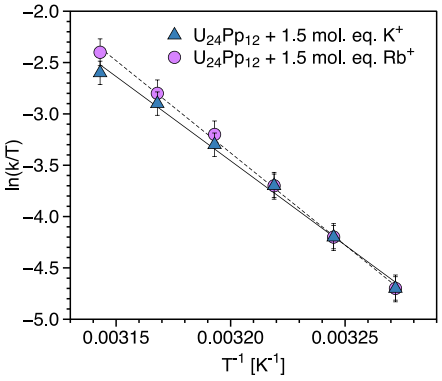

Figure 5. Eyring–Polanyi plot of the logarithm of rate versus temperature for the K^+- and Rb^+-titrated $\{U_{24}Pp_{12}\}$ solutions. The error bars indicate two standard errors obtained from a linear regression.

parameters were calculated as $\Delta H^{\ddagger} = 136 \pm 4$ kJ/mol and $\Delta S^{\ddagger} = 208 \pm 14$ J/mol·K for the K^+-containing system and as $\Delta H^{\ddagger} = 149 \pm 5$ kJ/mol and $\Delta S^{\ddagger} = 250 \pm 16$ J/mol·K for the Rb^+-containing system. These parameters represent an average between the three data sets (signals) because the same exchange process is occurring between the two conformations (O_h and D_{4h}), and the uncertainties are calculated from the standard error of regression. Overall, these values compare favorably to the data reported by Johnson et al. at 115 ± 3 kJ/mol $< \Delta H^{\ddagger} < 140 \pm 2$ kJ/mol and 163 ± 8 J/mol·K $< \Delta S^{\ddagger} < 223 \pm 7$ J/mol·K for $\{U_{24}Pp_{12}\}$ in the presence of Li^+, Na^+, and K^+.[19,21] These authors noted that the addition of TMA^+ cations to the $\{U_{24}Pp_{12}\}$ system resulted in stabilization of the D_{4h} conformation. The cause of this change was not clear, and potential diffusion of the TMA cation into the cavity of the cluster was postulated. In light of the current results that indicate a role for K^+ (and Rb^+) in triggering the O_h-to-D_{4h} transformation (Figures 1 and 2), we propose that the observed increase in the activation entropy upon the addition of TMA cations is caused by its ability to occupy and block the $\{U_6P_3O_9\}$ pores (Figure 3), preventing the departure of cations stabilizing the D_{4h} conformation, similar to the blocking role of guanidinium cations in the structure of $\{Mo_{132}\}$, rather than the direct interaction of TMA with the $\{U_{24}Pp_{12}\}$ cavity.[43]

The change in the magnetic environment between structurally unique Pp bridges of the $\{U_{24}Pp_{12}\}$ anion (as a Na/K salt, D_{4h}) was proposed to occur via conformational rearrangement involving a symmetrical (O_h) intermediate. In order for the Pp bridges to exchange positions without breaking bonds in the process, two trans-oriented $\{U_4\}$ units must change from *concave* to *convex*, while two different trans-oriented $\{U_4\}$ units change from *convex* to *concave* (Figure 6).

To elucidate the mechanism of conformational rearrangement, EXSY ^{31}P NMR measurements were conducted on a partially titrated Li/Na $\{U_{24}Pp_{12}\}$ system (K^+ mol equiv = 1.5) characterized by ca. 1:1 O_h/D_{4h} distribution of cluster

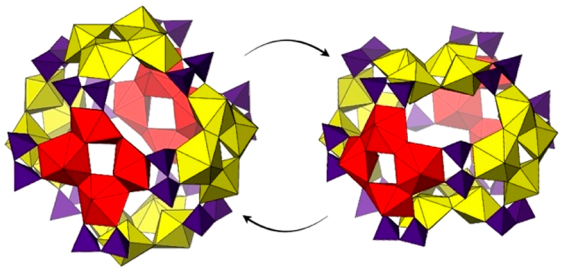

Figure 6. Polyhedral representation of D_{4h} $\{U_{24}Pp_{12}\}$ highlighting the concave-to-convex change of two trans-oriented $\{U_4\}$ units (red) during the magnetization-transfer process. Yellow and red polyhedra represent uranium peroxides, and purple polyhedra represent Pp bridges.

conformations (Table 1). Varying the mixing time (d8) from 5 to 300 ms resulted in the gradual emergence of cross-peaks, indicating magnetization transfer (Figure 7). At d8 = 5 ms, no cross-peaks were observed (Figure 7, left), indicating no transfer. At d8 = 40 ms, cross-peaks were noted between the signals corresponding to clusters in O_h and D_{4h} conformations (Figure 7, center, yellow arrows), and no cross-peaks were noted between D_{4h} signals. At d8 = 300 ms, cross-peaks between both the O_h and D_{4h} (Figure 7, right, yellow arrows) and D_{4h} signals (Figure 7, right, red arrows) were visible. EXSY ^{31}P NMR experiments conducted on the system containing Rb^+ (mol equiv = 3.1) showed similar cross-peak emergence behavior (Figure S9).

The results obtained from EXSY ^{31}P NMR experiments can be understood in terms of a mechanism by which magnetization transfer occurs without bond rupture but by swapping structural positions via an O_h intermediate. It is important to note that these experiments were conducted on a partially titrated system (K^+ and Rb^+ mol equiv = 1.5) and, as such, might not accurately describe the behavior of a pure system containing only the D_{4h} type of $\{U_{24}Pp_{12}\}$ clusters. Figure 8 illustrates two proposed magnetization-transfer mechanisms (*intramolecular* vs *intermolecular*), highlighting the role of K^+ (or Rb^+). The *intramolecular* and *intermolecular* pathways are distinct from one another based on whether the alkali-metal cations travel through the pores (*intermolecular*) or stay within the cavity of the cluster ion (*intramolecular*) undergoing conformational rearrangement.

The *intramolecular* exchange mechanism (Figure 8, top) involves movement of K^+ (or Rb^+) between their crystallographic sites *within* the cavity of the $\{U_{24}Pp_{12}\}$ cluster and possible release/uptake of other cations (Li^+ and Na^+) and water molecules. While Li^+, Na^+, and water molecules can move across the $\{U_6P_3O_9\}$ pores, their presence/absence does not affect the conformation of the $\{U_{24}Pp_{12}\}$ anion. We do not interpret these to have a significant impact on the proposed mechanism. *Intramolecular* exchange would result in retention of the D_{4h} conformation throughout the cation-shuffling process and subsequent magnetization transfer.

A second, *intermolecular* exchange mechanism (Figure 8, bottom) involves the release and uptake of K^+ (or Rb^+), resulting in a D_{4h}-to-O_h transition (upon the release of one or more K^+ or Rb^+) to the D_{4h} conformation (upon the uptake of one or more K^+ or Rb^+). For the *intermolecular* pathway, it is difficult to estimate the number of K^+ (or Rb^+) per $\{U_{24}Pp_{12}\}$ necessary to promote the O_h-to-D_{4h} change (and vice versa), but the titration results (Figure 1 and Table 1) showing the

https://dx.doi.org/10.1021/acs.inorgchem.9b03390
Inorg. Chem. 2020, 59, 2495–2502

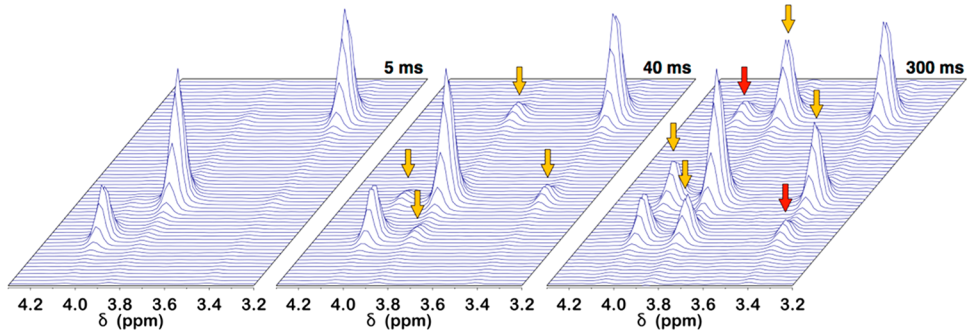

Figure 7. EXSY ^{31}P NMR spectra of partially titrated Li/Na $\{U_{24}Pp_{12}\}$ (K^+ mol equiv = 1.5) as a function of the mixing time (d8): (left) d8 = 5 ms; (center) d8 = 40 ms; (right) d8 = 300 ms. Yellow and red arrows highlight the cross-peaks between the O_h and D_{4h} and the D_{4h} and D_{4h} signals, respectively.

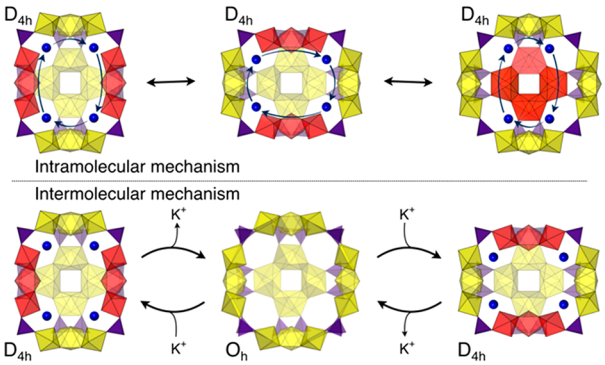

Figure 8. Polyhedral and ball representations of the intramolecular (top) and intermolecular (bottom) exchange of K^+ or Rb^+ within the $\{U_{24}Pp_{12}\}$ cluster (the front $\{U_4\}$ unit is not shown), leading to magnetization transfer between unique Pp bridges. Yellow, purple, and blue polyhedra/balls represent U, Pp, and K^+/Rb^+, respectively. Red polyhedra highlight concave $\{U_4\}$ units.

emergence of D_{4h} signals at $K^+/\{U_{24}Pp_{12}\}$ ratios of ca. 1:1 suggest that a single K^+ (or Rb^+) can, in principle, be sufficient. The emergence of cross-peaks between the O_h and D_{4h} clusters observed in EXSY ^{31}P NMR experiments (Figure 7) at shorter mixing times (d8 = 40 ms) supports an *intermolecular* exchange pathway in which conformational rearrangement involves the migration of K^+/Rb^+ from the cluster cavity to the bulk solution, and ultimately from one cluster to another. It is worth noting that the rates of solute diffusion between clusters cannot limit the rate of conformational rearrangement observed in the present study because the measured activation energies are too large: solute diffusion of these cations has activation enthalpies on the order of ca. 20 kJ/mol, which are much smaller than the values measured here experimentally. The rates of ion exchange have enthalpies slightly larger but also much less than the experimental activation enthalpies;[46] thus, it is likely that the rate-controlling step is the flex of the large ion architecture after ion exchange and not ion transport.

CONCLUSIONS

^{31}P NMR experiments have allowed for the first direct observation of the effect of K^+, Rb^+, and Cs^+ on the conformation of the $\{U_{24}Pp_{12}\}$ cluster. 1D NMR experiments revealed that the ion in solution formed by dissolution of the Li/Na salt of $\{U_{24}Pp_{12}\}$ exhibits an idealized O_h molecular symmetry but undergoes a conformational change to D_{4h} symmetry upon the addition of K^+ or Rb^+. The addition of Cs^+ to the system does not result in any apparent conformational change. Single-crystal X-ray diffraction studies confirm retention of the D_{4h} molecular symmetry in the systems titrated by K^+ or Rb^+ and reveal a new D_{2h} geometry of $\{U_{24}Pp_{12}\}$ in association with Cs^+.

The observation of titration cations within the cavity of the $\{U_{24}Pp_{12}\}$ clusters highlights the role of the cations in the process of the conformational change. Conformational rearrangement requires deformation of the $\{U_{24}Pp_{12}\}$ skeleton and is induced by cation−cluster interactions, highlighting the pliability of the Pp bridges. 1D VT ^{31}P NMR experiments showed increased activation enthalpy and entropy for the O_h-to-D_{4h} transformation in the presence of Rb^+ compared to K^+. 2D EXSY ^{31}P NMR experiments conducted on partially titrated K^+ and Rb^+ systems revealed that the magnetization transfer occurring between two unique Pp bridges present in the D_{4h} conformation of $\{U_{24}Pp_{12}\}$ occurs as K^+ or Rb^+ is taken up or released from its cavity. Overall, the results highlight the importance of counterion species in affecting the reactivities of actinide-based POMs and reveal that their impact on the solution dynamics of the $\{U_{24}Pp_{12}\}$ cluster is juxtaposed with their common description as "spectator ions".

ASSOCIATED CONTENT

Supporting Information

The Supporting Information is available free of charge at https://pubs.acs.org/doi/10.1021/acs.inorgchem.9b03390.

Crystal structures, ^{31}P NMR, ESI-MS, and Raman spectra, structure descriptions, and crystal data (PDF)

Accession Codes

CCDC 1966533−1966535 contain the supplementary crystallographic data for this paper. These data can be obtained free of charge via www.ccdc.cam.ac.uk/data_request/cif, or by emailing data_request@ccdc.cam.ac.uk, or by contacting The Cambridge Crystallographic Data Centre, 12 Union Road, Cambridge CB2 1EZ, UK; fax: +44 1223 336033.

AUTHOR INFORMATION

Corresponding Author

Peter C. Burns − *Department of Chemistry and Biochemistry and Department of Civil and Environmental Engineering and Earth Sciences, University of Notre Dame, Notre Dame, Indiana 46556, United States;* orcid.org/0000-0002-2319-9628; Email: pburns@nd.edu, prof.peter.c.burns@gmail.com

https://dx.doi.org/10.1021/acs.inorgchem.9b03390
Inorg. Chem. 2020, 59, 2495−2502

Authors

Mateusz Dembowski − *Department of Chemistry and Biochemistry, University of Notre Dame, Notre Dame, Indiana 46556, United States;* orcid.org/0000-0002-6665-8417

Corey D. Pilgrim − *Department of Chemistry, University of California, Davis, California 95616, United States*

Sarah Hickam − *Department of Civil and Environmental Engineering and Earth Sciences, University of Notre Dame, Notre Dame, Indiana 46556, United States*

Tyler Spano − *Department of Civil and Environmental Engineering and Earth Sciences, University of Notre Dame, Notre Dame, Indiana 46556, United States*

Dallas Hamlin − *Department of Civil and Environmental Engineering and Earth Sciences, University of Notre Dame, Notre Dame, Indiana 46556, United States*

Allen G. Oliver − *Department of Chemistry and Biochemistry, University of Notre Dame, Notre Dame, Indiana 46556, United States*

William H. Casey − *Department of Chemistry and Department of Earth and Planetary Sciences, University of California, Davis, California 95616, United States;* orcid.org/0000-0002-3275-6465

Complete contact information is available at: https://pubs.acs.org/10.1021/acs.inorgchem.9b03390

Notes

The authors declare no competing financial interest.

■ ACKNOWLEDGMENTS

This material is based upon work supported as a part of the Materials Science of Actinides Center, an Energy Frontier Research Center funded by the U.S. Department of Energy, Office of Science, Office of Basic Energy Sciences, under Award DE-SC0001089. NMR measurements were conducted at the Magnetic Resonance Research Center at the University of Notre Dame.

■ REFERENCES

(1) Burns, P. C.; Nyman, M. Captivation with Encapsulation: ADozen Years of Exploring Uranyl Peroxide capsules. *Dalton Trans.* **2018**, *47*, 5916−5927.

(2) Burns, P. C.; Kubatko, K. A.; Sigmon, G.; Fryer, B. J.; Gagnon, J. E.; Antonio, M. R.; Soderholm, L. Actinyl Peroxide Nanospheres. *Angew. Chem., Int. Ed.* **2005**, *44*, 2135−2139.

(3) Peruski, K. M.; Bernales, V.; Dembowski, M.; Lobeck, H. L.; Pellegrini, K. L.; Sigmon, G. E.; Hickam, S.; Wallace, C. M.; Szymanowski, J. E. S.; Balboni, E.; Gagliardi, L.; Burns, P. C. Uranyl Peroxide Cage Cluster Solubility in Water and the Role of the Electrical Double Layer. *Inorg. Chem.* **2017**, *56*, 1333−1339.

(4) Hickam, S.; Aksenov, S. M.; Dembowski, M.; Perry, S. N.; Traustason, H.; Russell, M.; Burns, P. C. Complexity of Uranyl Peroxide Cluster Speciation from Alkali-Directed Oxidative Dissolution of Uranium Dioxide. *Inorg. Chem.* **2018**, *57*, 9296−9305.

(5) Muller, A.; Gouzerh, P. From Linking of Metal-Oxide Building Blocks in a Dynamic Library to Giant Clusters with Unique Properties and Towards Adaptive Chemistry. *Chem. Soc. Rev.* **2012**, *41*, 7431−7463.

(6) Nyman, M.; Burns, P. C. A Comprehensive Comparison of Transition-Metal and Actinyl Polyoxometalates. *Chem. Soc. Rev.* **2012**, *41*, 7354−7367.

(7) Muller, A.; Krickemeyer, E.; Bogge, H.; Schmidtmann, M.; Peters, F. Organizational Forms of Matter: An Inorganic Super Fullerene and Keplerate Based on Molybdenum Oxide. *Angew. Chem., Int. Ed.* **1998**, *37*, 3359−3363.

(8) Muller, A.; Krickemeyer, E.; Meyer, J.; Bogge, H.; Peters, F.; Plass, W.; Diemann, E.; Dillinger, S.; Nonnenbruch, F.; Randerath, M.; Menke, C. $[Mo_{154}(NO)_{14}O_{420}(OH)_{28}(H_2O)_{70}]^{(25\pm5)-}$:A Water-Soluble Big Wheel with More Than 700 Atoms and a Relative Molecular-Mass of About 24000. *Angew. Chem., Int. Ed. Engl.* **1995**, *34*, 2122−2124.

(9) Hutin, M.; Rosnes, M. H.; Long, D. L.; Cronin, L. 2.10 Polyoxometalates: Synthesis and Structure − From Building Blocks to Emergent Materials. *In Comprehensive Inorganic Chemistry II* **2013**, 241−269.

(10) Qiu, J.; Burns, P. C. Clusters of Actinides with Oxide, Peroxide, or Hydroxide Bridges. *Chem. Rev.* **2013**, *113*, 1097−1120.

(11) Gao, N.; Sun, H. J.; Dong, K.; Ren, J. S.; Duan, T. C.; Xu, C.; Qu, X. G. Transition-Metal-Substituted Polyoxometalate Derivatives as Functional Anti-amyloid Agents for Alzheimer's Disease. *Nat. Commun.* **2014**, *5*, 5.

(12) Kamata, K.; Yonehara, K.; Sumida, Y.; Yamaguchi, K.; Hikichi, S.; Mizuno, N. Efficient Epoxidation of Olefins with ≥ 99% Selectivity and Use of Hydrogen Peroxide. *Science* **2003**, *300*, 964−966.

(13) Busche, C.; Vila-Nadal, L.; Yan, J.; Miras, H. N.; Long, D. L.; Georgiev, V. P.; Asenov, A.; Pedersen, R. H.; Gadegaard, N.; Mirza, M. M.; Paul, D. J.; Poblet, J. M.; Cronin, L. Design and Fabrication of Memory Devices Based on Nanoscale Polyoxometalate Clusters. *Nature* **2014**, *515*, 545−549.

(14) Wylie, E. M.; Peruski, K. M.; Weidman, J. L.; Phillip, W. A.; Burns, P. C. Ultrafiltration of Uranyl Peroxide Nanoclusters for the Separation of Uranium from Aqueous Solution. *ACS Appl. Mater. Interfaces* **2014**, *6*, 473−479.

(15) Burns, P. C.; Ewing, R. C.; Navrotsky, A. Nuclear Fuel in a Reactor Accident. *Science* **2012**, *335*, 1184−1188.

(16) Banerjee, A.; Bassil, B. S.; Roschenthaler, G. V.; Kortz, U. Diphosphates and Diphosphonates in Polyoxometalate Chemistry. *Chem. Soc. Rev.* **2012**, *41*, 7590−7604.

(17) Kortz, U. Polyoxometalate-diphosphate Complexes. 5. Cigar-shaped 30-molybdobispyrophosphate: Structure of $(N(C_4H_9)_4)_2H_9[\{(P_2O_7)Mo_{15}O_{45}\}_2][PMo_{12}O_{40}]$. *Inorg. Chem.* **2000**, *39*, 623−624.

(18) Ling, J.; Zhang, H. X.; Qiu, J.; Stoffer, M.; Burgess, D.; Burns, P. C. Pyrophosphate and Methylenediphosphonate Incorporated Uranyl Peroxide Cage Clusters. *Cryst. Growth Des.* **2018**, *18*, 7720−7729.

(19) Johnson, R. L.; Ohlin, C. A.; Pellegrini, K.; Burns, P. C.; Casey, W. H. Dynamics of a Nanometer-Sized Uranyl Cluster in Solution. *Angew. Chem., Int. Ed.* **2013**, *52*, 7464−7467.

(20) Dembowski, M.; Colla, C. A.; Hickam, S.; Oliveri, A. F.; Szymanowski, J. E. S.; Oliver, A. G.; Casey, W. H.; Burns, P. C. Hierarchy of Pyrophosphate-Functionalized Uranyl Peroxide Nanocluster Synthesis. *Inorg. Chem.* **2017**, *56*, 5478−5487.

(21) Dembowski, M.; Olds, T. A.; Pellegrini, K. L.; Hoffmann, C.; Wang, X. P.; Hickam, S.; He, J. H.; Oliver, A. G.; Burns, P. C. Solution ^{31}P NMR Study of the Acid-Catalyzed Formation of a Highly Charged $\{U_{24}Pp_{12}\}$ Nanocluster, $[(UO_2)_{24}(O_2)_{24}(P_2O_7)_{12}]^{48-}$, and Its Structural Characterization in the Solid State Using Single-Crystal Neutron Diffraction. *J. Am. Chem. Soc.* **2016**, *138*, 8547−8553.

(22) Gao, Y. Y.; Dembowski, M.; Szymanowski, J. E. S.; Yin, W. B.; Chuang, S. S. C.; Burns, P. C.; Liu, T. B. A Spontaneous Structural Transition of $\{U_{24}Pp_{12}\}$ Clusters Triggered by Alkali Counterion Replacement in Dilute Solution. *Chem. - Eur. J.* **2017**, *23*, 7915−7919.

(23) Misra, A.; Kozma, K.; Streb, C.; Nyman, M. Beyond Charge Balance: Counter-Cations in Polyoxometalate Chemistry. *Angew. Chem., Int. Ed.* **2020**, *59*, 596.

(24) Sures, D.; Segado, M.; Bo, C.; Nyman, M. Alkali-Driven Disassembly and Reassembly of Molecular Niobium Oxide in Water. *J. Am. Chem. Soc.* **2018**, *140*, 10803−10813.

(25) Hou, Y.; Nyman, M.; Rodriguez, M. A. Soluble Heteropolyniobates from the Bottom of Group IA. *Angew. Chem., Int. Ed.* **2011**, *50*, 12514−12517.

(26) Nyman, M. Polyoxoniobate Chemistry in the 21st Century. *Dalton Trans.* **2011**, *40*, 8049−8058.

(27) Fullmer, L. B.; Mansergh, R. H.; Zakharov, L. N.; Keszler, D. A.; Nyman, M. Nb_2O_5 and Ta_2O_5 Thin Films from Polyoxometalate Precursors: A Single Proton Makes a Difference. *Cryst. Growth Des.* **2015**, *15*, 3885−3892.
(28) Xuan, W. M.; Pow, R.; Watfa, N.; Zheng, Q.; Surman, A. J.; Long, D. L.; Cronin, L. Stereoselective Assembly of Gigantic Chiral Molybdenum Blue Wheels Using Lanthanide Ions and Amino Acids. *J. Am. Chem. Soc.* **2019**, *141*, 1242−1250.
(29) Zhao, J. W.; Li, Y. Z.; Chen, L. J.; Yang, G. Y. Research Progress on Polyoxometalate-based Transition-Metal-Rare-Earth Heterometallic Derived Materials: Synthetic Strategies, Structural Overview and Functional Applications. *Chem. Commun.* **2016**, *52*, 4418−4445.
(30) Miro, P.; Pierrefixe, S.; Gicquel, M.; Gil, A.; Bo, C. On the Origin of the Cation Templated Self-Assembly of Uranyl-Peroxide Nanoclusters. *J. Am. Chem. Soc.* **2010**, *132*, 17787−17794.
(31) Vlaisavljevich, B.; Gagliardi, L.; Burns, P. C. Understanding the Structure and Formation of Uranyl Peroxide Nanoclusters by Quantum Chemical Calculations. *J. Am. Chem. Soc.* **2010**, *132*, 14503−14508.
(32) Miro, P.; Vlaisavljevich, B.; Gil, A.; Burns, P. C.; Nyman, M.; Bo, C. Self-Assembly of Uranyl-Peroxide Nanocapsules in Basic Peroxidic Environments. *Chem. - Eur. J.* **2016**, *22*, 8571−8578.
(33) Liu, G.; Liu, T. B.; Mal, S. S.; Kortz, U. Wheel-shaped Polyoxotungstate $[Cu_{20}Cl(OH)_{24}(H_2O)_{12}(P_8W_{48}O_{184})]_{25}$-Macroanions Form Supramolecular "Blackberry" Structure in Aqueous Solution. *J. Am. Chem. Soc.* **2006**, *128*, 10103−10110.
(34) Liu, T. B.; Langston, M. L. K.; Li, D.; Pigga, J. M.; Pichon, C.; Todea, A. M.; Muller, A. Self-Recognition Among Different Polyprotic Macroions During Assembly Processes in Dilute Solution. *Science* **2011**, *331*, 1590−1592.
(35) Soltis, J. A.; Wallace, C. M.; Penn, R. L.; Burns, P. C. Cation-Dependent Hierarchical Assembly of U_{60} Nanoclusters into Macro-Ion Assemblies Imaged via Cryogenic Transmission Electron Microscopy. *J. Am. Chem. Soc.* **2016**, *138*, 191−198.
(36) Boskovic, C. Rare Earth Polyoxometalates. *Acc. Chem. Res.* **2017**, *50*, 2205−2214.
(37) Patel, A.; Narkhede, N.; Singh, S.; Pathan, S. Keggin-type Lacunary and Transition Metal Substituted Polyoxometalates as Heterogeneous Catalysts: A Recent Progress. *Catal. Rev.: Sci. Eng.* **2016**, *58*, 337−370.
(38) Long, D. L.; Burkholder, E.; Cronin, L. Polyoxometalate Clusters, Nanostructures and Materials: From Self Assembly to Designer Materials and Devices. *Chem. Soc. Rev.* **2007**, *36*, 105−121.
(39) Krause, L.; Herbst-Irmer, R.; Stalke, D. An Empirical Correction for the Influence of Low-Energy Contamination. *J. Appl. Crystallogr.* **2015**, *48*, 1907−1913.
(40) Sheldrick, G. M. SHELXT - Integrated Space-Group and Crystal-Structure Determination. *Acta Crystallogr., Sect. A: Found. Adv.* **2015**, *71*, 3−8.
(41) Sheldrick, G. M. Crystal Structure Refinement with SHELXL. *Acta Crystallogr., Sect. C: Struct. Chem.* **2015**, *71*, 3−8.
(42) Muller, A.; Das, S. K.; Talismanov, S.; Roy, S.; Beckmann, E.; Bogge, H.; Schmidtmann, M.; Merca, A.; Berkle, A.; Allouche, L.; Zhou, Y. S.; Zhang, L. J. Trapping Cations in Specific Positions in Tuneable "Artificial Cell" Channels: New Nanochemistry Perspectives. *Angew. Chem., Int. Ed.* **2003**, *42*, 5039−5044.
(43) Muller, A.; Krickemeyer, E.; Bogge, H.; Schmidtmann, M.; Roy, S.; Berkle, A. Changeable Pore Sizes Allowing Effective and Specific Recognition by a Molybdenum-Oxide Based "Nanosponge": En Route to Sphere-Surface and Nanoporous-Cluster Chemistry. *Angew. Chem., Int. Ed.* **2002**, *41*, 3604−3609.
(44) Evans, M. G.; Polanyi, M. Some Applications of the Transition State Method to the Calculation of Reaction Velocities, Especially in Solution. *Trans. Faraday Soc.* **1935**, *31*, 875−893.
(45) Eyring, H. The Activated Complex in Chemical Reactions. *J. Chem. Phys.* **1935**, *3*, 107−115.
(46) Nyman, M.; Alam, T. M. Dynamics of Uranyl Peroxide Nanocapsules. *J. Am. Chem. Soc.* **2012**, *134*, 20131−20138.

https://dx.doi.org/10.1021/acs.inorgchem.9b03390
Inorg. Chem. 2020, 59, 2495−2502